MNRAS **000**, 1–8 (2021) Preprint 15 August 2021 Compiled using MNRAS LATEX style file v3.0

N-body simulation
the solar system and swing-by maneuver in Newtonian gravity

Florian Hilpert, [1] Martin Beyer, [2] Sebastian Gratz [3]
[1] *Friedrich-Schiller Universität Jena* ⋆
[2] *Friedrich-Schiller Universität Jena* †
[3] *Friedrich-Schiller Universität Jena* ‡

15 August 2021

ABSTRACT

This is a review on creating a n-body simulation and implementing a swing-by maneuver where we restrict to the sun and the planets of the solar system as well as one space probe in the swing-by part as point-like masses in Newtonian gravity.
In this paper we consider the implementation of the solar system and compare different integrators (forward Euler, Runge-Kutta and leap-frog method) with respect to their accuracy and convergence behaviour. Further we consider the dependence on the aimed error. Secondly we consider the implementation of a swing-by maneuver at Jupiter using the example of the New Horizons mission and determine the dependence of the minimum distance to Jupiter on the variation of initial angle with respect to the ecliptic plane and starting velocity.

Overall, we were able to produce an accurate simulation of the solar system for 248 years using the Cash-Karp method. This appears to be a necessary tool for weighting numerical errors with numerical cost to end up at both: appropriate integration times and good approximations. Based on that it was possible to simulate direct flights to other planets as well as swing-by maneuvers for Jupiter and Saturn. The success of these maneuvers hugely depends on the initial conditions which have to be determined carefully.

Key words: gravitation – celestial mechanics – methods: numerical

⋆ florian.hilpert@uni-jena.de
† m.beyer@uni-jena.de
‡ sebastian.gratz@uni-jena.de

1 INTRODUCTION

Astronomical n-body simulations are one of the primary tools to model the movement of large astronomical objects with an appropriate scaling. As the technologies for space exploration develop, it is already a vital tool for planning and calculating journeys to extraterrestrial objects. Despite significant hardware improvements, there are limitations on the accuracy of such simulations. All methods are limited by their numerical errors. In order to do numerical simulations one resorts to highly efficient codes. As this paper will show the chosen simulation method has a significant impact on the final probe trajectory. Furthermore the used algorithms simulate a direct probe flight from Earth to different planets in our solar system, as well as a swing-by maneuver.

2 CHOICE OF INTEGRATOR SCHEMES

In order to find differences of explicit and symplectic integrator schemes we chose to implement the explicit forward Euler scheme and the symplectic leap-frog method. In computational simulations the accuracy of the results must be weighted against the numerical cost. Important markers are the convergence properties of the integrators, the accuracy and the suitable step size needed, which determines the speed of the code. The simulation shall, as is also physically reasonable, leave quantities like energy and angular momentum conserved.

Since both methods have the disadvantage that they converge only to low order (first order for Euler and second order for leap-frog) we chose to implement the Runge-Kutta-4 (RK4) scheme which is an explicit integrator scheme converging to fourth order.

Having not just a solar system to implement but also space probes starting from a planet it is necessary to run the code with different time scales for the sake of efficiency, where short step sizes have to be used near planets and larger ones if the probe is far out in space and no quick changes in velocity happen. Therefore we chose to implement and for all simulations work with the more sophisticated Cash-Karp (CK) method which compares integration results of two embedded Runge-Kutta schemes converging to fourth and fifth order. The difference Δ in the solution of both integrators is then of order $O\left(\mathrm{d}t^5\right)$. For a given error of size Δ_0 we should have used a step size of

$$\mathrm{d}t_{\mathrm{new}} = \mathrm{d}t_{\mathrm{old}} \left|\frac{\Delta_0}{\Delta}\right|^{\frac{1}{5}}. \tag{1}$$

This means after every integration step the step size is adapted matching the given error Δ_0. Thus the CK-method lowers the step size if necessary and enlarges it if possible. A table with the necessary prefactors can be found in W.H. Press et al. (1992).

In order to check if the integrator schemes were implemented correctly the behaviour of the numerical error can be considered as the step size decreases. W.l.o.g. assuming that the integrator has a formal order of convergence of $O(h^n)$ the error should decrease with the step size due to a power law: $f(h) = m \cdot h^n$, which can be rephrased in terms of a linear function in a log-log (error - step size) plot as follows:

$$f'(h) \equiv \log\left(\frac{f(h)}{m}\right) = n \cdot \log(h) = n \cdot h'. \tag{2}$$

Thus the log-log plot should show a linear correspondence between error and step size with an ascend equal to the order of convergence n.

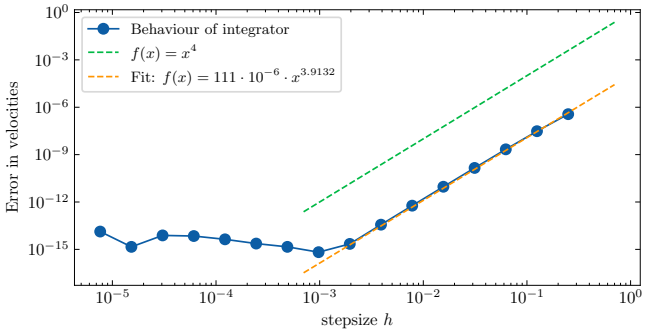

Figure 1. Convergence behaviour of the Runge-Kutta-4 method for integration of the negative sine function.

To check the correct implementation numerically the negative sine function has been used as a test function which had to be integrated by the routines. Since the acceleration function of the n-body problem is vector valued the test integration has been done for all cartesian components. The results of the different components agreed exactly and thus the graphs were done only for the first component. To determine the real order of convergence a fit $f(x) = a \cdot x^b$ has been used for all integrator schemes. Because the RK4-method is used for integration later on its result is given in figure 1. Here we can see the correct convergence behaviour of fourth order which is also approximately met by the fitted function. Furthermore we notice the characteristic behaviour of integrator schemes, namely that if the step size decreases far enough the error increases again due to the amount of numerical calculations that have to be performed. Interestingly and in contrast to the forward Euler method, the numerical error approaches the region of machine accuracy already at rather large step sizes, which could also be noticed for both integrator parts in the CK-method. Further description and graphs of the convergence behaviour of the other integrator schemes can be found in the appendix.

All of the implemented integrator schemes (forward Euler, RK4, leap-frog and CK) show the correct convergence behaviour we expected, which leads us to assume that they were implemented correctly and we can use them for further simulations.

3 MODELLING THE SOLAR SYSTEM

As initial data for the solar system we used Folkner et al. (2014) supplying data for June 28, 1969 in the ICRF2 frame. For simplicity we picked this frame for numerical calculations where the coordinate origin is the center of mass at initial time $t = 0$. Although the center of mass has a non-vanishing momentum in this frame and thus is not fixed, it barely varies for one orbit of Pluto which is the largest period we ever consider. We have further limited ourselves to implement only the sun, the planets and Pluto.

3.1 Numerical implementation of gravity a n-body interaction

The basic idea for building and simulating a solar system as an n-body system is that the interactions can be broken down to two-body interactions for which the third Kepler law holds:

$$\text{const.} = \frac{T^2}{a^3} = \frac{4\pi^2}{G(M_\odot + m)} \overset{M_\odot \gg m}{\approx} \frac{4\pi^2}{GM_\odot}. \tag{3}$$

The law simply states that the ratio of T^2 and a^3 is a global constant for the planets of the solar system where the constant can be determined considering Earth. Since it is convincing in terms of the

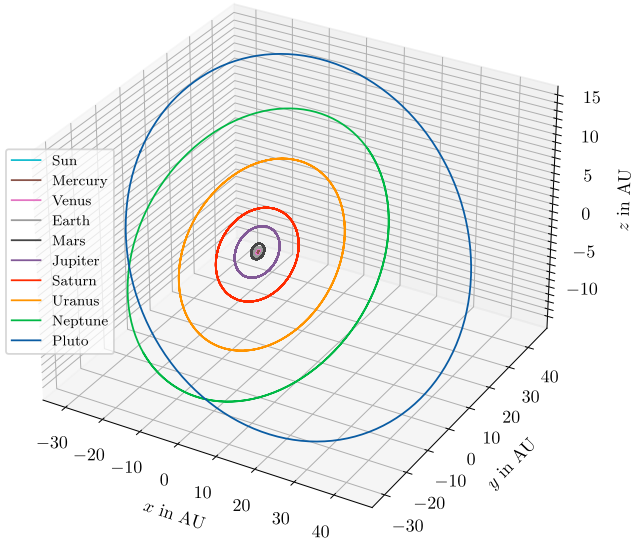

Figure 2. Trajectories for the solar system for a period of 248 years in three dimensions. The orbit of Pluto is tilted with respect to the ecliptic plane which lies mainly in the xy-plane.

distance and time scales to be considered we work in astronomical units (AU) for distances and years (yr) for times, where we have $T = 1$ yr and $a = 1$ AU for Earth and thus the global constant becomes $1\,\mathrm{yr}^2/\mathrm{AU}^3$. Therefore the Kepler law simplifies to $GM \approx 4\pi^2\,\mathrm{AU}/\mathrm{yr}^2$ and Newton's law of gravity becomes

$$\vec{F} = -\frac{GM_\odot m}{r^3}\vec{r} \approx -\frac{4\pi^2 m}{r^3}\vec{r} \tag{4}$$

which can be rewritten in components of acceleration of the i-th body due to the j-th body

$$\vec{a}_{ij} \approx -\frac{4\pi^2(\vec{r}_i - \vec{r}_j)\ \mathrm{AU}^3/\mathrm{yr}^2}{\sqrt{(\Delta x_{ij})^2 + (\Delta y_{ij})^2 + (\Delta z_{ij})^2}^3} \qquad \Delta w_{ij} \equiv w_i - w_j. \tag{5}$$

To avoid division by zero we define $a_{ii} := 0$ which simply means that a body does not accelerate by itself. Calculating the n-body solar system therefore comes down to evaluating all $n(n-1)/2$ different two-body interactions and summing up all contributions for each body in order to arrive at the next (intermediate) time step and add contributions of several intermediate steps in a more sophisticated way to end up at the next time step with higher accuracy.

Following this idea and running the simulation for one orbit of Pluto one gets the trajectories of figure 2, where one notices that all the planet orbits lie approximately in a common plane, the ecliptic plane, and just the orbit of Pluto is significantly inclined against it.

3.2 Numerical analysis

Looking at the energies of the solar system presented in figure 3 we notice from the continuous lines that the kinetic as well as the potential energy oscillate with a frequency that corresponds to the orbiting time of Jupiter as the largest contribution which is marked by thin vertical lines. A second contribution with a frequency corresponding to the orbiting time of Saturn, marked by thicker vertical lines, arises as can be seen from the periodicity of the dashed lines which are kinetic and potential energy if the solar system is evolved without Jupiter. The total energy of the system however stays constant as it is expected of a closed system and is negative which shows that the system is gravitationally bound.

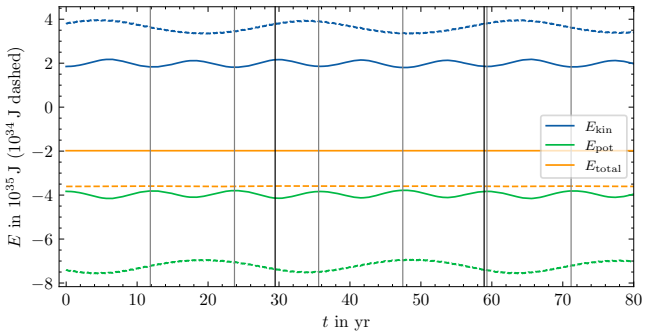

Figure 3. Comparison of solar system energies. The dashed lines indicate the energies without Jupiter. It can be seen that the periodicity of the kinetic and potential energy is dominated by the orbital periods of Jupiter (11.86 yr) and Saturn (29.46 yr). Note the different energy scaling for solid and dashed lines.

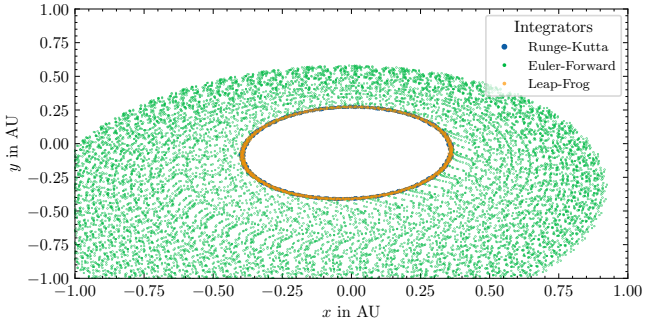

Figure 4. Calculated trajectories of Mercury for an integration time of 248 yr. While the Runge-Kutta and Leap-frog form stable solutions, the forward-Euler scheme gains energy over time.

Now we investigate the behaviour of different integrator schemes on the solar system and compare explicit methods (Euler-forward and Runge-Kutta) with symplectic methods (leap-frog). For the analysis we use the orbit of Mercury since its orbital velocity is the highest in the solar system and thus it is most prune to numerical errors in the integration scheme. We test the integration methods for a fixed step size of $\mathrm{d}t = 1.5 \cdot 10^{-5}$ year ≈ 8 min and a time period of 248 years. The step size was chosen such that the error of the RK4-scheme is at the order of machine accuracy. The results of the various integration schemes are illustrated in figure 4. Note that not every calculated data point is displayed. As expected the forward Euler scheme is not energy conserving as Mercury seems to gain energy over time and taking an orbit similar to Earth. For the RK4- and leap-frog-scheme we do not observe a substantial difference.

Now we switch back to the CK-method of adapting the integration step size for a given error in the integration. Using the RK4-scheme we again integrate the trajectory of Mercury for 100 years. This was done in figure 5. We observe that a given error of $\Delta_0 = 10^{-10}$ AU is already sufficient to correctly integrate the trajectory of a planetary system for at least a century. However, for objects on which large accelerations act, a smaller error is needed to obtain the correct trajectory. Small changes of the initial condition of a space probe at launch may lead to large deviations in the final trajectory. Thus, in the following we will choose a desired error of $\Delta_0 = 10^{-18}$ AU.

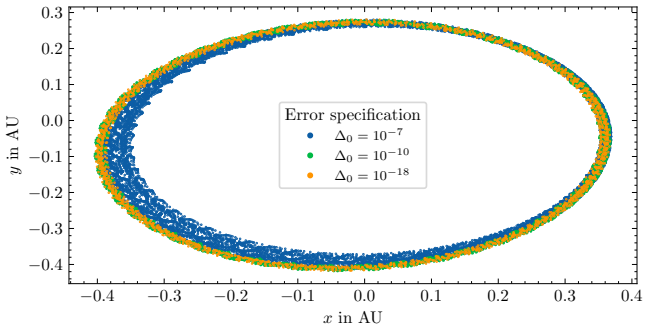

Figure 5. Calculated trajectories of Mercury for an integration time of 100 years for different errors Δ_0 using the CK-method. Between $\Delta_0 = 10^{-18}$ AU and $\Delta_0 = 10^{-10}$ AU no deviation in the trajectories is visible, whereas for $\Delta_0 = 10^{-7}$ AU the error gets too large.

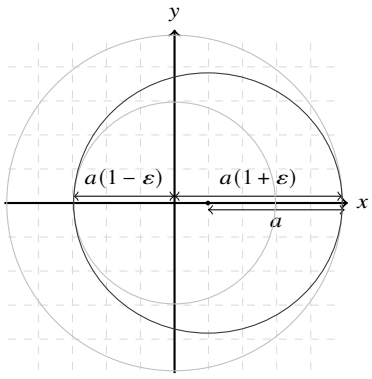

Figure 6. Determine the returning interval $a \cdot (1-\varepsilon) \leq d \leq a \cdot (1+\varepsilon)$ of a space probe for the orbit of Pluto (thicker line).

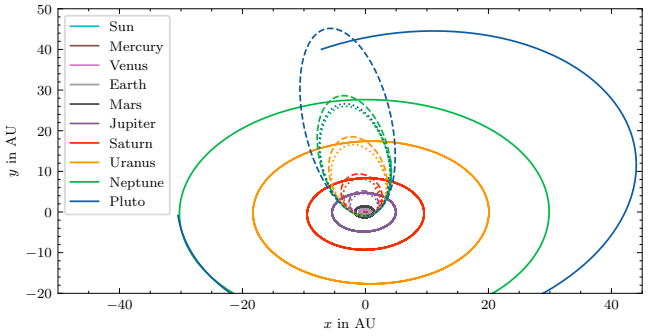

Figure 7. Trajectories for probes corresponding to calculated minimal and maximal initial velocity starting from Earth to different outer bodies.

4 DIRECT FLIGHT TO BODIES

One of our goals was to implement a space probe that is sent out on a planet and reaches a target body or at least the region of the Kepler orbit where the body resides. We wanted to have a fully numerical approach that does not depend on an analytical approximation. For simplicity in this and all further simulations just the initial conditions for the bodies and space probes are set and once done the system is evolved in time without any course corrections for the probe. The space probe starts at the surface of the starting-object with an absolute initial velocity without being accelerated first to reach it. By the notion of an absolute velocity the velocity with respect to the origin of the ICRF2 frame is meant. The space probes are treated as mass-less test objects of vanishing radius and the bodies are treated as spheres, where for their radii and orbit parameters we used data from the planet fact sheets in Williams (2019) collected in table A1. In order avoid problematic small distances of space probes and planets a crash function checks whether a probe is closer to a body than its radius. It then crashes and is eliminated from further calculations.

Reaching a body directly is done in three steps: first we have to find the interval of absolute initial velocity for the probe to return close to the region of the targets orbit and remember the relative velocity to the start-object, since it varies during one of its years. Secondly we adjust the starting time to come close to the target body and finally modify the part of the velocity perpendicular to the ecliptic plane in order to actually reach a body whose orbit is tilted a bit with respect to the ecliptic.

The developed algorithm should be capable of calculating the interval of absolute velocity for a space probe starting from any planet to any outer body meaning that e. g. Mars to Earth would not be possible but Earth to Mars is.

4.1 Calculating the interval of absolute velocity

To reach planets directly the space probe is demanded to return at a distance d which lies between the smallest and largest distance of the target body from the origin $a(1-\varepsilon) \leq d \leq a(1+\varepsilon)$, which is the region where the planet can be found as can be seen from figure 6. That means finding values of the initial velocity which correspond to a maximal probe distance of $a \cdot (1-\varepsilon)$ and $a \cdot (1+\varepsilon)$. All the velocities in between are assumed to be good to reach the target planet directly.

The algorithm that determines them works as follows:
After setting start object and target, the orbit parameters a and e of the target are read in and the maximal and minimal returning distance is calculated. For the initial velocity the value of $v = 10\,\mathrm{AU/yr}$ was picked which is above the solar escape velocity from earth. Ten space probes with evenly distributed velocities from 1 to 10 AU/yr pointing in the direction of the movement of the start-object are initialized and set in front of the planet at the distance of its radius to start directly from the surface in the direction of motion as it is done for real launches in order to save energy. The solar system with all probes is evaluated for a sufficiently long period for the space probes to reach the target. During the time evolution we keep track of the velocity and the distance to the origin of each space probe to check whether they returned in the sought distance interval. After the evolution we check what the minimal velocity was for each probe and how far they were from the origin when they had that velocity. If those distances are not inside the interval the velocities have to be refined and we initialize 100 probes with velocities from 0.1 to 10.0.

If a velocity is inside (e.g. 9.0 and 9.1) the algorithm looks how far the interval can be extended and initializes 20 probes: 10 below the lowest and 10 above the highest velocity for which the maximal distance was inside the interval. Now we have two intervals with refined velocities (e.g. 8.91 up to 9.00 for the lower velocity limit and 9.10 up to 9.19 for the higher velocity limit). Successively the algorithm tries to calculate the velocity limits to higher accuracy, up to a certain decimal place which was set in the beginning and finally shows both calculated values.

For different target planets the velocity interval was calculated as shown in table A2. The velocity algorithm refused service for Neptune thus the values represented are the closest values where the algorithm said 'too low' and 'too high' meaning that the corresponding probes returned too close or too far from the origin. Manual adjustments were performed to find the appropriate starting velocities for Neptune. In figure 7 the trajectories for probes with the calculated initial velocities are shown.

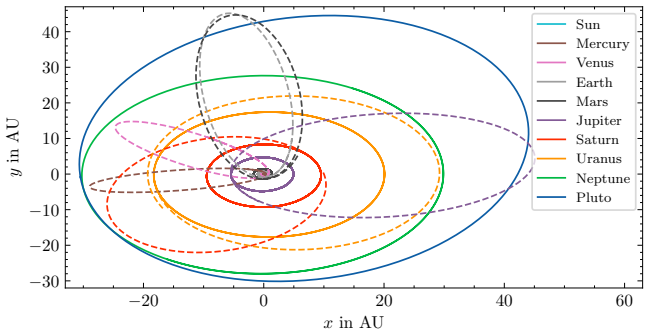

Figure 8. Trajectories for probes sent to Plutos orbit from different planets of the solar system (dashed lines). The plots were chosen from both the lower and the upper velocity limit. For reasons of clarity only one of them is displayed for each planet.

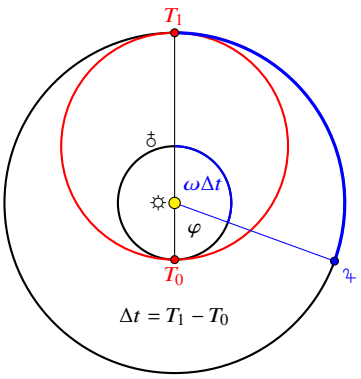

Figure 9. Schematics for an analytical estimate of the starting angle φ for a Hohmann-transfer between earth ♁ and Jupiter ♃. Using the Hohmann-transfer time Δt and the angular velocity $\omega = 2\pi/T$ (c. f. table A1) of the planet the starting angle between Earth and the target planet is given by $\varphi = \pi - \omega\Delta t$.

Furthermore we also want to generalize the algorithm for different starting planets now looking for trajectories towards Pluto. Here the interval of absolute velocity has been calculated as well (c. f. table A3). However, the algorithm refused service starting from Jupiter. The presented values for the gas giants were found manually and are presented in figure 8. Note that for Plutos rather elliptical trajectory, reaching the orbit is a challenging task. For example consider the Uranus trajectory. Here the probe reached the nearly circular orbit of Neptune which also intersects Plutos orbit. Even though the Uranus trajectory completely misses Plutos real trajectory, the distance is actually correct. For Neptune the calculation was omitted since its trajectory lies partially in Plutos orbit.

4.2 Optimizing the starting time and velocity

As we have seen in the previous section, the launch time of the space probe is important, especially when we want to reach the planet and not just its trajectory. At first we need to know at which time the probe has to be sent from earth in order to interact with the planet. We estimate the starting time analytically using Keplers third law, which can be used to calculate the time T of a Hohmann-transfer

$$\frac{T^2}{a^3} = \frac{4\pi^2}{GM_\odot} \Rightarrow \Delta t = \frac{T}{2} = \frac{1}{2}\sqrt{\frac{4\pi^2 a^3}{GM_\odot}}, \quad \text{with} \quad a = \frac{a_♁ + a_♃}{2}. \tag{6}$$

Now we can determine the angle between earth and the target planet at the time of launch using the illustration in figure 9. We assume a circular planetary orbit where the space probe intersects with the planet after half a period of the Hohmann-transfer.

Now we simply integrate the planets until the condition of $\varphi = \pi - \omega\Delta t$ is met. Since there exist two planetary configurations with the same angle we also demand that φ should decrease with increasing time. This calculation is not perfect, since the planetary orbits are not circular, however the first estimate gives the correct starting time within a time span of 0.1 year. Now we can use an algorithm to further adjust the first estimate of the starting time. For a first velocity estimate we use the minimum velocity values calculated in section 4.1. A step-wise increase of velocity is then used to minimize the distance between probe and target planet. The numerical scheme can be applied to all outer planets in the solar system. The results are shown in figure 10. The algorithm is able to send the probe to within 0.1 AU of the target planet. For Pluto, however, the estimate is worse since its orbital plane is tilted (c. f. figure 2).

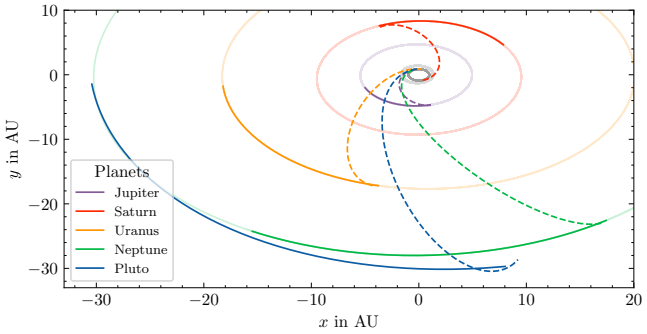

Figure 10. Calculated trajectories (dashed lines) of probes starting from Earth towards different planets of the solar system.

4.3 Adjusting the ecliptic angle

The planets (except for Pluto) move approximately in the ecliptic plane. In order for a space probe to closely approach a target body that does not lie in exactly the same plane as the start-object, the part of the probes initial velocity perpendicular to the ecliptic plane has to be adjusted in order to minimize the distance of the probe to the target body measured perpendicular to the ecliptic plane. We assume that the relation between perpendicular velocity and perpendicular distance is given by an affine function: $d^\perp(v^\perp) = m \cdot v^\perp + n$. As is evident from figure 2 the normal part of the initial velocity vector standing perpendicular on the ecliptic plane encloses a small angle φ with the $z-$axis and thus we have

$$v_z \quad = \quad \cos\varphi \cdot v^\perp \overset{\varphi \text{ small}}{\approx} v^\perp. \tag{7}$$

A similar relation holds for the z-component of the distance d_z and the perpendicular distance $d^\perp$ such that we can use instead of the perpendicular distance the z-distance function depending on the z-component of the velocity instead of the perpendicular part:

$$d^\perp(v^\perp) = m \cdot v^\perp + n \qquad \mapsto \qquad d_z(v_z) = m \cdot v_z + n. \tag{8}$$

Then we launch the current probe another one with slightly different v_z component and get two different points, each a tuple (v_z, d_z). From those two points we can find the zero point $d_z(v_z) = 0$ of the approximated affine function and thus the perpendicular velocity which minimizes the perpendicular distance to first order.

5 THE SWING-BY MANEUVER

Realizing a swing-by maneuver works except for a few more steps quite similarly to the direct flight method. In order to gain energy from the planet, the space probe must pass the planet from behind. This means for the optimization process it is advantageous to start at velocities that are too high rather than too low. For the transfer and starting time we use again the values for direct flight calculated in section 4.2. We assume that the starting time is kept fixed and optimize by this assumption the starting angle with respect to the ecliptic plane. This results in a new z-component of the probes initial velocity. After that, the velocity of the probe is optimized using a more sophisticated approach which gets along with a rough estimate of the starting velocity as a first input. This reduces the distance perpendicular to the ecliptic plane.

5.1 Adjusting the ecliptic angle

This step works the same as in the direct approach case except for the fact that the two trajectories have to be chosen such that they pass behind Jupiter in order for the probes to gain energy from the swing-by. Then launching two probes with slightly different velocity z-components and calculating a new one with the angle adjusting routine for the space probe that reduces the distance is exactly the same as before. However, this adjustment was only necessary for the trajectory to Pluto since the other planets are moving in the ecliptic plane. Therefore this optimization part was omitted for the other planets, since it did not improve the results.

5.2 Adjusting the velocity

In order to adjust the velocity in the ecliptic plane we assumed a parabolic dependence of the distance d on the absolute initial velocity of the probe. This assumption was based on simulations with Jupiter, one of which is displayed in figure 11. We need a trajectory behind Jupiter for which we start three probes: the one we already have and two with slightly larger and smaller absolute velocity. We obtain three tuples of probe velocity and the planets ecliptic distance. From those we can determine the minimum of the planets distance in the ecliptic plane with points (v_1, d_1), (v_2, d_2) and (v_3, d_3) by a formula found here Brünner (2003):

$$v_{\min} = \frac{1}{2}\frac{v_2^2(d_3-d_1) - v_1^2(d_3-d_2) - v_3^2(d_2-d_1)}{v_2(d_3-d_1) - v_1(d_3-d_2) - v_3(d_2-d_1)}. \tag{9}$$

This gives the optimized velocity to second order. Then we can perform a fine search in an interval $v_{\min} \pm 0.1\,\mathrm{AU/yr}$ to find the minimum velocity. The velocity dependence for these intervals is shown in figure 11. For most planets the minimum lies in the middle of the interval, which indicates, that this first estimate was already coming close to the desired minimum.

5.3 Modelling New Horizons

In order to verify the integration method and test the optimizing algorithm we used the trajectory of the interplanetary space probe New Horizons which was launched on January 19, 2006 by NASA with an initial velocity of $16.26\,\mathrm{km\,s^{-1}}$ Scharf (2013). We used these initial conditions to start a probe at Earths radius with this initial relative speed (with respect to Earth). The resulting trajectory is displayed in figure 12.

However, during the flight towards Jupiter the velocity of New Horizons was adjusted several times by thrusters correcting the trajectory. This may be one reason why the integrated trajectory does not reach Pluto after 9.5 years (the fly-by was on July, 14 2015). Furthermore, slight deviations from the starting position and velocity change the final trajectory dramatically since the minimum distance to Jupiter during the swing-by maneuver is very important. In order to improve the starting trajectory, we fixed the launch date and made adjustments to the direction and magnitude of the starting velocity using the algorithms described in section 5.1 and 5.2. Using these methods the minimal distance to Jupiter could be reduced to 10^6 km. This matches the minimal distance of the New Horizons trajectory of $2.3 \cdot 10^6$ km well JHU (2007). However, this new trajectory still misses Pluto by a large amount. This is probably due to the lack of swing-by maneuvers also performed on Uranus and Neptune in the original mission.

We also examined the absolute velocity of the space probe as a function of time as shown in figure 13. Here we observe, that the velocity for the trajectory calculated by the original starting data was reduced during the swing-by since the probe passed Jupiter from the front. Therefore the probe did not reach solar escape velocity. This problem was avoided in the algorithm by starting at larger velocities and minimizing the distance by a step-wise reduction of starting velocity leading to swing-by trajectories behind Jupiter. Then we observe a velocity increase of $\Delta v \approx 3.79\,\mathrm{km\,s^{-1}}$ which corresponds well to the New Horizons mission of $3.890\,\mathrm{km\,s^{-1}}$ JHU (2007).

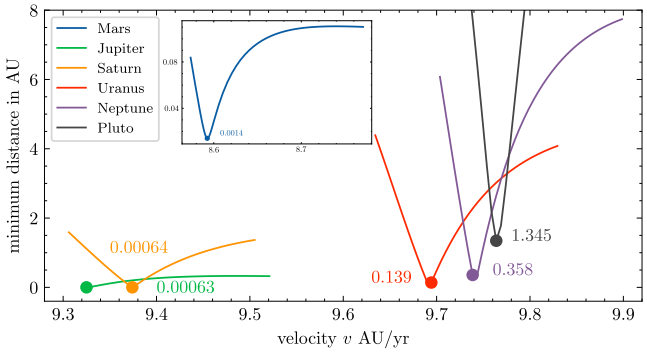

Figure 11. Dependence of minimum distance between space probe and the target planet on the initial probe velocity. For the initial considerations the dependence looked to be parabolic, however, investigations for the outer planet show, that the assumption of a linear dependence might have been sufficient.

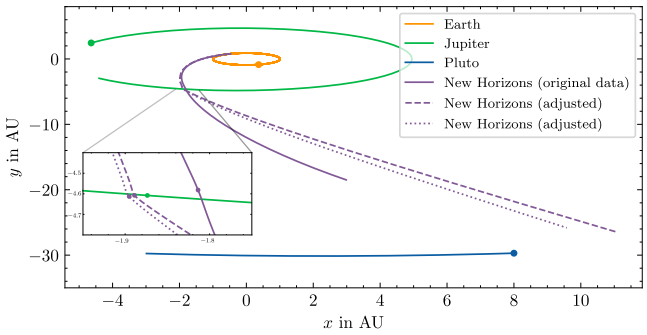

Figure 12. The trajectory of the New Horizons interplanetary space probe integrated with the initial conditions (start time January 19th, 2006) and velocity ($16.26\,\mathrm{km\,s^{-1}}$). The dashed (dotted) lines show an improved trajectory by first adjusting the starting velocity (angle) and then optimizing the angle (velocity). We observe that for the original data, the space probe would transit in front of Jupiter leading to a deceleration.

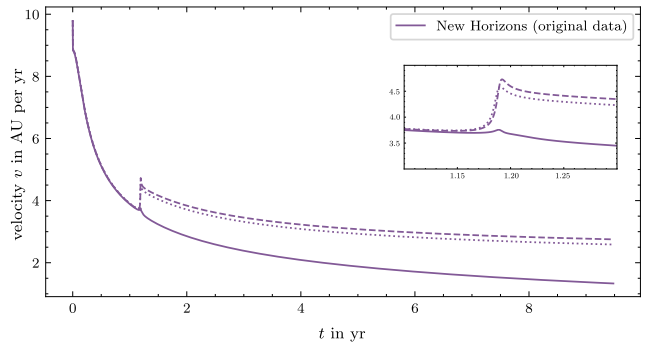

Figure 13. The absolute velocity of the New Horizons interplanetary space probe as a function of time. For the adjusted trajectories we observe an energy gain due to the successful swing-by maneuver. For calculations using the original starting conditions, the space probe is decelerated by Jupiter.

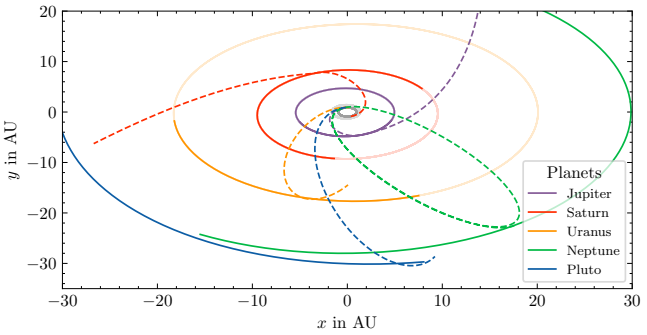

Figure 14. Trajectories of space probes for swing-by maneuvers at the planets. A significant energy gain was only obtained for the swing-by maneuvers at Jupiter and Saturn where the minimal distance was about 96 000 km which is 1.5 times the radius of Jupiter.

5.4 Application to custom space probes

We now want to apply the swing-by maneuver to custom space probes with the goal to achieve a successful swing-by maneuver for each planet individually. However, due to the larger distance and lower masses, a swing-by maneuver with Uranus, Neptune or Pluto is rather difficult to achieve. The latter is particularly challenging, since its orbit is tilted with respect to the ecliptic requiring extra care. We use the starting times acquired in section 4 for the direct flight to the planets and take the calculated velocity as the first initial condition. We now apply the same algorithms which were performed on the New Horizons probe to the other planets of the solar system. The results are shown in figure 14. We observe, that successful swing-by maneuvers were only realized for Jupiter and Saturn, which is probably due to their high masses. The minimum distances to the planets can be found in figure 11 and are nearly the same for the Jupiter and Saturn trajectory with $d_{\min} \approx 96\,000\,\mathrm{km}$. These trajectories are presumably as good as technologically possible with real space probes because the distance is only one and a half times the radius of Jupiter.

We also analyzed the energy gain of the swing-by maneuvers at Jupiter and Saturn. The absolute velocity of the space probe is shown in figure 15. For Jupiter we observe a velocity increase of $\Delta v = 2.6\,\mathrm{AU/yr} \approx 12.3\,\mathrm{km\,s^{-1}}$. This is approximately the velocity of New Horizons when it will reach a distance of 100 AU in 2038 Buckley (2006).

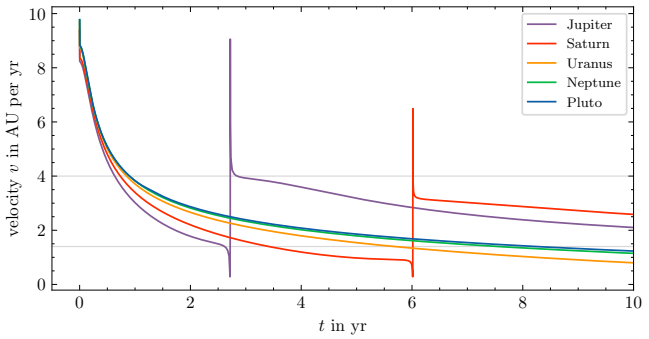

Figure 15. Energies of space probes for swing-by maneuvers at different planets. Trajectories of space probes for swing-by maneuvers at the planets. The largest velocity increase was achieved for Jupiter with $\Delta v = 2.6\,\mathrm{AU/yr}$.

6 CONCLUSION AND OUTLOOK

The numerical analysis showed that applying the CK-method is the preferred method for a n-body simulation. We observe that the error of position should be less than 10^{-15}. We used this algorithm to simulate the n-body dynamics of the solar system using all planets and Pluto mutually interacting gravitationally. Furthermore we implemented a scheme of starting a space probe at arbitrary planets and sending it to outer planets. For that we wrote an algorithm optimizing the velocity in the ecliptic plane and the starting angle with respect to the ecliptic plane. The success of the implementation was shown by optimizing the flight of the New Horizons space probe, realizing a swing-by maneuver with a velocity increase comparable to the original mission. Then we applied the scheme to find other possible trajectories for a swing-by maneuver and successfully achieved them for a flight to Jupiter and Saturn which lead to velocity increases above any space mission of our knowledge. However the algorithm is just able to perform a single swing-by maneuver. We would have to further optimize the algorithm with additional parameters to achieve multi swing-by maneuvers such as the Voyager 2 mission in 1977 with a total of four swing-by's. For that we would suggest the implementation of a simplex algorithm which is better suited for the minimization problem, where different parameters such as starting time and velocity components can be adjusted simultaneously.

REFERENCES

Brünner A., 2003, Quadratische Funktion durch 3 Punkte finden, https://www.arndt-bruenner.de/mathe/10/parabeldurchdreipunkte

Buckley M., 2006, New Horizons Salutes Voyager, https://web.archive.org/web/20141113224847/http://pluto.jhuapl.edu/news_center/news/081706.php

Folkner W. M., Williams J. G., Boggs D. H., Park R. S., Kuchynka P., 2014, Interplanetary Network Progress Report, 42-196, 47

JHU 2007, Pluto-Bound New Horizons Spacecraft Gets a Boost from Jupiter, https://web.archive.org/web/20141113224828/http://pluto.jhuapl.edu/news_center/news/022807.php

Scharf C. A., 2013, The Fastest Spacecraft Ever?, https://blogs.scientificamerican.com/life-unbounded/the-fastest-spacecraft-ever/

W.H. Press S.A. Teukolsky W.T. Vetterling B.P. Flannery 1992, Numerical Recipies in C, 2. edn edn. Cambridge University Press

Williams D. R., 2019, Planetary Fact Sheet - Metric, https://nssdc.gsfc.nasa.gov/planetary/factsheet/

Table A1. Orbit parameters taken for calculations and radii of the bodies for initial positions, crash-checking and starting time calculation.

Body	a / AU	ε	r / 10^{-3}AU	T / yr
Mercury	0.387	0.2056	0.01630	0.24101
Venus	0.723	0.0068	0.04045	0.61562
Earth	1.0	0.0167	0.04263	1.00000
Mars	1.524	0.0935	0.02270	1.88085
Jupiter	5.204	0.0489	0.47788	11.862
Saturn	9.583	0.0565	0.40286	29.447
Uranus	19.201	0.0457	0.17084	84.016
Neptune	30.048	0.0113	0.16553	164.79
Pluto	39.237	0.2488	0.00794	247.94

Table A2. Intervals of absolute and relative velocities for space probes starting from Earth to different bodies at initial time $t = 0$.

Target	$v_{\min} / \frac{\text{AU}}{\text{yr}}$	$v_{\max} / \frac{\text{AU}}{\text{yr}}$	$v^{\text{rel}}_{\min} / \frac{\text{AU}}{\text{yr}}$	$v^{\text{rel}}_{\max} / \frac{\text{AU}}{\text{yr}}$
Mars	8.5889	8.6628	2.4093	2.4832
Jupiter	9.1719	9.2317	2.9923	3.0521
Saturn	9.3833	9.4187	3.2037	3.2391
Uranus	9.5388	9.5561	3.3592	3.3765
Neptune	9.5996	9.6096	3.4200	3.4300
Pluto	9.6021	9.6467	3.4225	3.4671

Table A3. Intervals of absolute and relative velocity to the start-object for space probes going to Pluto starting from different planets at initial time $t = 0$.

Start	$v_{\min} / \frac{\text{AU}}{\text{yr}}$	$v_{\max} / \frac{\text{AU}}{\text{yr}}$	$v^{\text{rel}}_{\min} / \frac{\text{AU}}{\text{yr}}$	$v^{\text{rel}}_{\max} / \frac{\text{AU}}{\text{yr}}$
Mercury	14.4477	14.4847	4.1255	4.1625
Venus	11.0100	11.0517	3.6692	3.7109
Earth	9.6021	9.6466	3.4225	3.4670
Mars	7.4409	7.5045	2.1498	2.2134
Jupiter	15.1980	15.2205	12.5734	12.5959
Saturn	9.5923	9.6018	7.4982	7.5077
Uranus	5.9964	6.0225	4.4935	4.5001
Neptune	—	—	—	—

APPENDIX A: APPENDIX

The following figures describe the convergence behaviour of the error for the integration of the negative sine function. For the forward Euler scheme the convergence behavior is linear as expected. The fitted function confirms the linear convergence as can be seen in figure A1. Even for small step sizes the error is quite large. For the leap-frog method a convergence behaviour of second order could be verified by the fitted function which was expected (c.f. figure A2). One also notices that the error is quite large and it takes small step sizes to have an error near to the machine accuracy but is still off by several orders of magnitude.

For both integrators of the CK-method we see in figures A4 and A3 that they converge as expected to fourth and fifth order, which could be verified by the fitted functions. For both schemes the error increases if the step size gets too small due to the amount of numerical calculations that have to be performed. Both schemes have a minimal error close to the machine accuracy where the fifth-order part is closer than the fourth-order part and the errors are quite small already at larger step sizes.

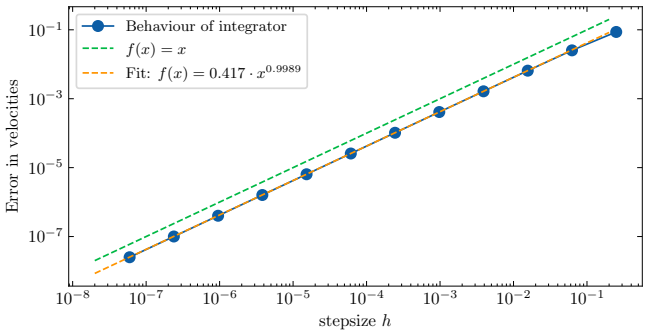

Figure A1. Convergence behaviour of the forward Euler method.

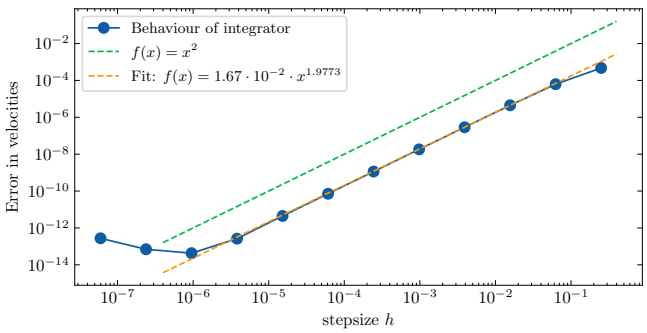

Figure A2. Convergence behaviour of the leap-frog method.

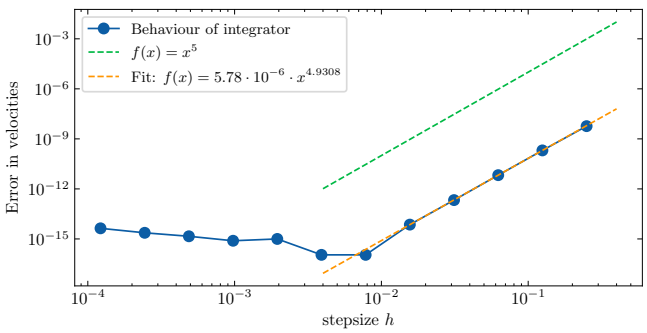

Figure A3. Convergence behaviour of the RK5 part of the Cash-Karp method.

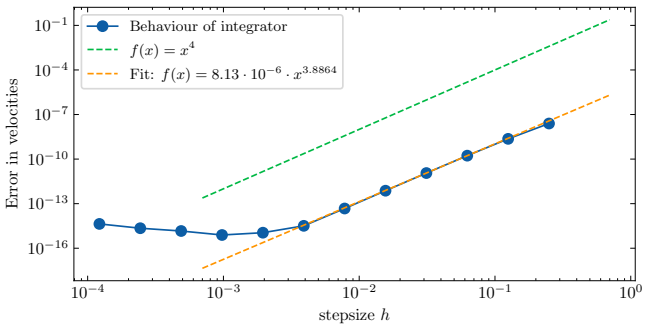

Figure A4. Convergence behaviour of the RK4 part of the Cash-Karp method.